Proceedings of the 9th International Conference on Cyclotrons and their Applications
September 1981, Caen, France

STATUS OF THE CHALK RIVER SUPERCONDUCTING HEAVY-ION CYCLOTRON

J.H. Ormrod, C.B. Bigham, E.A. Heighway, C.R. Hoffmann, J.A. Hulbert and H.R. Schneider

Atomic Energy of Canada Limited
Research Company
Chalk River Nuclear Laboratories
Chalk River, Ontario K0J 1J0

Abstract.- The Chalk River four-sector K=520 superconducting cyclotron is designed to accelerate all ions from lithium (to 50 MeV/u) to uranium (to 10 MeV/u) using a 13 MV tandem Van de Graaff as injector[1]. After an extended shutdown the magnet has been reassembled and field measurements resumed. During the shutdown a ground fault between the superconducting coil and its container was removed, the flutter poles were shimmed and the remaining trim rod holes were bored in them, the 104 trim rods with their holders were installed and the cryostat inner wall was modified to accept the radiofrequency accelerating structure. Experiments on the radiofrequency accelerating system, cryopumps, electrostatic deflector and superconducting windings for the magnetic channel are done in separate test chambers. Recent results and the status of all subsystems are given.

1. Introduction.- The tandem-cyclotron heavy-ion accelerator facility is shown in Fig. 1. Negative ions are accelerated to 300 keV from one of the ion sources and before entering the tandem Van de Graaff pass through a low energy buncher that gives a time focus at the tandem terminal. The first bending magnet beyond the tandem is used for energy analysis and charge-state selection. A high energy buncher is located at a focus between the second and third bending magnets. Slits beyond the next bending magnet provide the feedback signal for setting the phase of the low energy buncher. The final two bending magnets upstream of the cyclotron are used for matching the cyclotron dispersion to provide the required beam phase-space orientation at the stripping foil located in a dee near the center of the cyclotron. A small dipole in the cyclotron yoke wall provides the final steering to direct the beam onto this foil at the correct radius. Four dees, interleaved with the flutter poles, operate at 100 kV peak and accelerate the beam to the extraction radius of 650 mm where a single electrostatic deflector directs the beam into a magnetic channel composed of iron bars and superconducting windings that provide both adjustable bias and adjustable focusing. The Y-magnet downstream of the cyclotron is used for energy analysis (except when the beam is directed to the ISOL - on line isotope separator) and to connect the tandem beamline to the experimental area when the beamline that bypasses the cyclotron is used.

Project funding is divided into two phases. The first phase, now approved, includes the required building additions and all components necessary to bring the beam beyond the Y-magnet and will provide minimum target locations. Funding for the second phase, which we hope will follow the first without hiatus, provides for the new scattering target equipment, the beam line to it and the other existing target rooms and the second ion source shown dashed in the figure.

A more detailed description of the extraction system[2] appears elsewhere in these proceedings. Progress on the other cyclotron subsystems is detailed below.

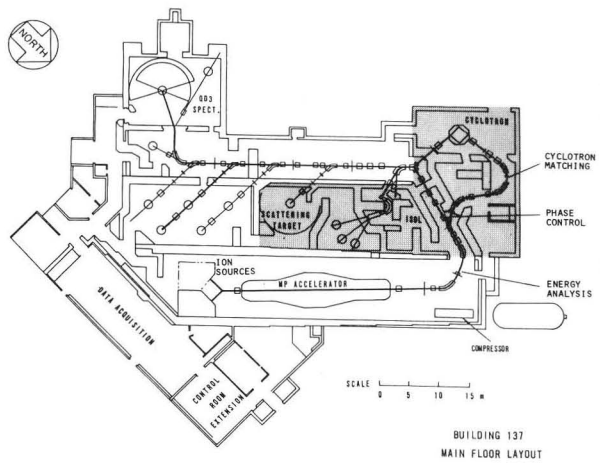

Fig. 1 Plan view of the facility.

2. Elimination of Coil Ground Fault.- Towards the end of the third cooldown period, after more than a month of field mapping runs, short circuits developed near the midplane in the upper coil. These short circuits did not affect the coil operation but invalidated many diagnostic readings. It is now believed, that despite care taken, fragments of stainless steel fell into the coil container during its initial closing when two stainless steel bellows had to be cut from the top of the container and replaced.

Initially the shield segments and superinsulation were removed from the regions where resistance measurements suggested that the shorts were located, and then these regions were studied by x-ray 'shadowgraph' using a 20 Ci Iridium 192 source. No coil winding displacements could be detected. A 19 mm diameter hole was trepanned in the 6 mm wall of the upper helium vessel near an x-ray shadow in a magnet cooling slot. The shadow was found to be caused by a non-shorting pellet of 304 stainless steel weld rod 'splash' but near the same spot, grinding debris was

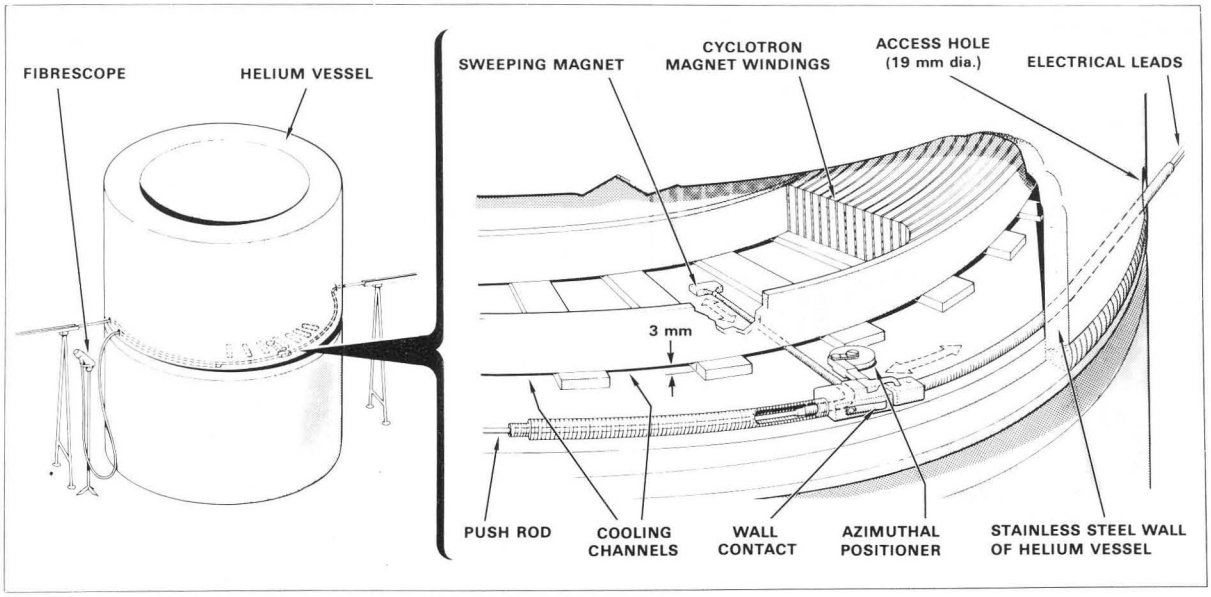

Fig. 2 Illustration of the apparatus used to remove the ferromagnetic debris from the coil.

picked up which, although 18-8 stainless material, was nevertheless ferromagnetic because it had been cut by grinding with a 'dental' burr. During coil excitation this debris could collect along lines of induction and bridge the 3 mm gap between the helium vessel midplane base and the innermost coil pancake.

A full scale model of a section of the midplane cooling channels was made and used to develop a tool that could move round the 25 mm wide space between the coil and the outside wall of the helium vessel at the coil midplane circumference and clean out each of the 96 midplane cooling channels in turn. Each channel is tapered from 45 to 30 mm wide, 185 mm deep and just under 3 mm high. A constraint was placed on the tool that it should require the minimum number of access holes and the holes should be no larger than the 19 mm 'spy' hole already cut.

Figures 2 and 3 show the final form of the tool. A brass head carried two spring contacts which gave an electrical indication when the head was pushed tightly into the angle of the helium vessel wall. A roller, on a knuckle, also fitted with an electrical contact, indicated the location of the head relative to the channel spacers. The head could be moved around the coil circumference by two opposing 4 m lengths of steel spring helix, 5 mm in outside diameter. Down the centre of the right-hand helix ran the wiring for the electrical position indicators and the left-hand helix carried the actuator for the cleaning head. The sweeping was done with an Alnico magnet on the end of a 200 mm spring arm. The spring arm could be ejected from and retracted into a magazine in the left-hand helix by a long beryllium-copper push rod running through the helix.

Three access holes were needed to assemble the cleaning tool inside the helium vessel and to operate it. One of the holes also served as a port for fragment removal and for viewing operations with a fibrescope. Special short tools had to be made to clean channels partly obscured by coil leads. Access for these special tools was possible because the access locations had been chosen near the lead positions.

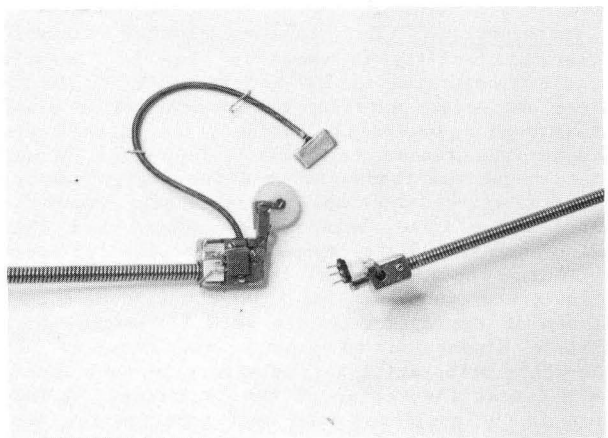

Fig. 3 Tool head of the coil cleaning apparatus.

After three cleaning runs, subjecting the winding to external magnetic disturbances with a large electromagnet between runs to 'shake' loose any trapped debris, no more debris could be found. The total amount of debris removed from the coil was 140 milligrams and the final coil resistance to ground was in excess of 3000 MΩ at 300 V dc.

The three access holes were closed with welded plugs and the shield and superinsulation replaced. The coil was again brought up to full field in March 1981 and many times since. The short circuits have not recurred.

3. Cryostat Modification.- The superconducting cyclotron development was initiated as two model studies, one for the magnet system, the other for the rf accelerating structure. Thus at the early stages, those aspects of the magnet design relating to the attachment of the rf structure were planned but not necessarily implemented. In the case of the magnet coil cryostat, ports were left in the outer wall of the vacuum casing for probes, beam lines and so on, but were blanked off and not extended through the mid-

plane. The inner wall was shaped in radial profile and left unperforated.

After the field mapping and field stability tests were concluded in the summer of 1979 it was necessary to complete the cryostat to make room at the midplane for dee clearance.

The vacuum casing was removed and while the coil cleaning was proceeding as described above, five large apertures were machined in the inner wall. Four of these were required to accept copper segments which form part of the rf cavity wall and bulge into the cryostat to provide a minimum of 38 mm of radial dee clearance. The fifth aperture was to allow the end of the extraction channel to protrude into the rf cavity.

A typical section of the completed wall is shown in Fig. 4. The light coloured tape covers the smooth finish where the midplane vacuum seal rings will seat. One complete copper segment is seen, clamped with square clips into its O-ring sealed port. The oval tube entering the segment is for the injected beam, and now passes completely through the midplane of the cryostat to the outer wall. Immediately to the left is the smaller cover plate for the extraction channel access. This plate replaces the extraction channel cover during field mappping to allow free azimuthal motion of the flip coil assembly. The vertical clamp between the two plates is recessed at the midplane to give clearance to the extracted beam. To the right of the dished copper segment is a section of the original cryostat wall, copper plated and bored, under the round cover plate, for a flag probe which will be used to check the beam alignment before entry to the extraction channel. Another of the four dee clearance segments may be seen in part, further to the right. The clips will be covered by rf finger stock, held down by the narrow strips visible in the figure.

Tests on the rf structure in its dummy vacuum tank showed that the cryostat inner wall may absorb up to 2 kW of rf power. The five large apertures are cooled around their edges with water lines which run down to a manifold inside the cryostat vacuum. Tests on one fitted segment showed that 500 W could be absorbed without the O-ring seal temperature exceeding 100°C.

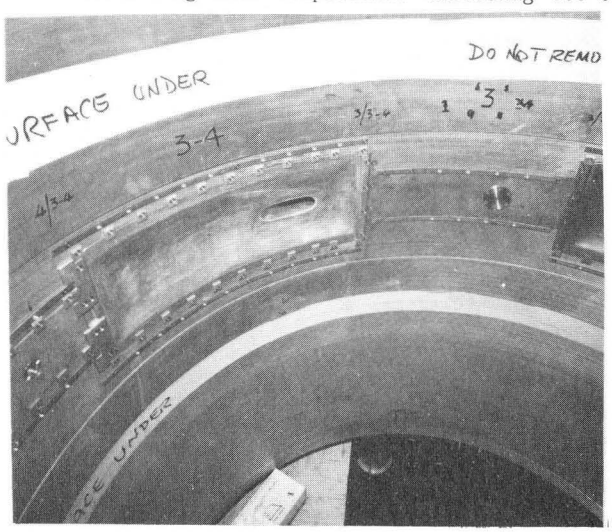

Fig. 4 The cryostat inner wall showing one of the bulged copper segments that face an accelerating dee. The oval aperture is the inboard termination of the injection hole.

The superinsulation is protected from excess heating by a 3 mm aramid felt lining inside each copper segment. Thirty-two temperature sensors (Analog Devices Inc. AD590) monitor the rf dissipation in the copper segments and around the intervening cryostat wall areas.

At the current stage of modification the cryostat has midplane penetrations fitted for both radial probes and the injected beam. Remaining to be fitted are the extraction channel and its electrical leads and the penetration for the flag probe.

Initially, the heat leak into the helium bath at zero coil current was 11 watts, and 14 watts at full field. Following the modifications described, the heat leak rose to 16 W at zero current. Much of this increase is probably related to the extensive superinsulation patching after the coil cleanup and may be recoverable by a full renewal of the superinsulation. The addition of the extraction channel is expected to increase the heat loading by a further 3-5 watts.

4. Cryopumps.- The midplane region of the cyclotron must be maintained at a pressure $\sim 5 \times 10^{-7}$ torr (70 μPa) to minimize charge exchange losses of the accelerated beam. Two upper valleys have been chosen as sites for cryopumps and access holes left through the poles for cryofeeds. Moderate rf currents flow in the valleys and special care must be taken to shield the pump refrigerant from rf heating.

A 'MK I' pump was designed to use as much of the valley floor area as practicable, and a minimum of valley height because of dee-ground capacitance restrictions. This pump has operated for over 150 hours during rf cavity tests. It has two thermal/rf baffles, the outer one (valley floor) water cooled and the inner one, operating at 80 K, cooled by the boil-off helium with a heat leak at cavity half power (50 kW) of only 0.4 W to the liquid helium. No other refrigeration is required beside the supply of liquid helium at 0.6 $\ell \cdot h^{-1}$. The small liquid capacity, due to the valley height restriction, necessitates a helium filling every 60 minutes. With the transfer tube used (20 layers of superinsulation in vacuum) transfer losses exceed boil-off losses by a factor 3-4 but are expected to be reduced considerably when the transfer tube is replaced by one with an internal radiation shield. Vacuum fluctuations from temperature excursions of the intermediate baffle occurred during initial operation but are now eliminated by refilling before the helium pool completely evaporates.

The MK I pump has a speed of 320 ℓs^{-1} for air (a factor 2½ below that ultimately required). The rf attenuation at each pump baffle is estimated at 14-16 dB.

The MK II pump being prepared for initial tests is expected to have a speed of 900-1000 ℓs^{-1}. The redesigned baffles should have a similar rf attenuation to those of the MK I pump. Relaxation of the dee-ground capacitance restriction has permitted the use of a larger liquid helium tank with an expected boil-off time of 4-5 hours.

5. Bunchers.- Bunching of the dc beam from the ion source is accomplished using two rf bunching cavities. The low energy buncher has a gridded (1 mm spacing) 1 mm gap to achieve a satisfactory transit time factor for the heaviest ions. The ideal sawtooth wave form is approximated by a fundamental and first harmonic

rf voltage up to a peak value of 2 kV. The rf voltage is produced by coaxial $\lambda/4$ capacitively tuned resonators in the same cavity with the beam passing along the axis and through the gridded gap at one end. Both fundamental and harmonic rf drive power are provided by a single broad band solid state amplifier. Phase and amplitude controls are provided at low level before the amplifier.

The high energy buncher must perturb a higher energy beam and hence requires a much larger voltage. The required voltage is reduced by using a drift tube, 2 gap buncher and operating it at the 2nd or 4th harmonic. A single drift tube on a quarter-wave resonator tuned with a sliding short is adequate for all beams by using the 4th harmonic for cyclotron harmonic number h=2 beams and the 2nd harmonic for h=4 and h=6 beams. The buncher must then be tuned from 62 MHz to about 200 MHz and the drift length is about 65 mm. The maximum peak voltage required is about 20 kV and the rf power $\approx$ 200 W. Frequency multiplication, phase and amplitude control are in the low level drive line.

6. Rf Structure and Controls.- The rf accelerating system is a structure with two coupled resonators having opposite dees on coaxial tuners above and below the midplane on the axis of the cyclotron, each tuner being adjusted to resonance with a sliding short. This system, tuned to either the "in-phase" resonance or the "out-of-phase" resonance and the appropriate cyclotron harmonic, covers the full energy range with a one octave tuning range, 31 to 62 MHz. This gives a compact structure largely inside the cyclotron magnet all driven by one rf feed[3].

The structure is being operated in a dummy vacuum vessel so that high power testing may be carried out separately from the magnet development. Full voltage has been attained over most of the frequency range but the rf contacts on the main tuners have not demonstrated satisfactory reliability. The outer conductors of the tuners have also had to be redesigned and rebuilt. Controls, monitor circuits and computer interface circuits are under development and the system has been operated under computer control. A block diagram of the system is shown in Fig. 5. Current work is concentrated on the main tuner contact problem.

The original design was a sliding tuner operating continously under power so that temperature transients could be followed at fixed drive frequency. The first contacts used were small doubled back beryllium copper fingers. These worked up to full voltage but subsequently failed because their spring range was not large enough to cover the variations in the tuner dimensions. The second type of contact was also beryllium copper but longer to cover the tuner dimensional variations. These failed at about two thirds of full voltage. Current work is on the long finger type made out of a higher conductivity copper alloy (CDA Alloy No. 155) and on the development of an alternative clamping short.

The rf drive signal is derived from a stable frequency synthesizer and passes through a low level modulator to the input of the power amplifier chain comprised of a broad band solid state amplifier to the 400 W level, a cavity-tuned triode driver to the 7 kW level and a cavity-tuned tetrode output stage to the 100 kW level. The output is transmitted by a 50 Ω line to the rf drive capacitor which is adjustable to maintain a matched load over the frequency range.

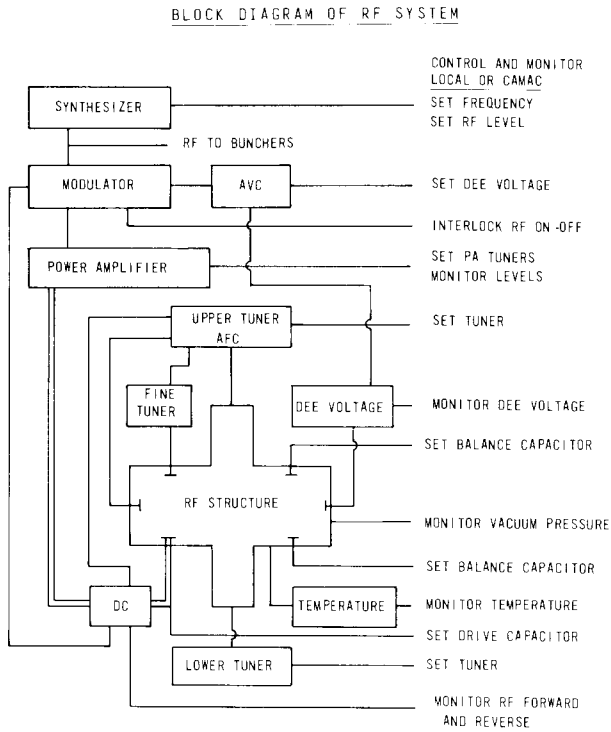

Fig. 5 Block diagram of the rf system showing the control and monitoring connections for either local or computer control.

The modulator protects the power amplifier from mismatches on the output by turning off the drive if the reverse power goes above a set level. The structure multipactors at less than 1 W drive and must generally be driven hard to the 50 kW level to break through. To accomplish this, the modulator turns the rf on hard for 50 μs. If the reverse signal goes low, the rf stays on; if the reverse stays high indicating multipactoring (or mistuning) the rf switches off for 0.1 seconds and then comes on again. The cw rf level is controlled by the automatic voltage control which balances the dee voltage probe signal against the dee voltage set level. The modulator also turns off the rf for tuner movements or vacuum transients.

Both tuners, the rf drive capacitor and balance capacitors are set initially for the desired frequency from tuning curves. The upper tuner (for the driven resonator) may be switched to an automatic frequency controller which uses the phase of the forward power and the dee voltage to keep the dees on resonance. The fine tuner is also operated from this signal and reduces the number of main tuner motions required.

The dee voltages are monitored by two capacitor probes at each dee giving a total of 8 rf signals. The rf signals are rectified and read out separately. They are also summed to give averages for each resonator and for both resonators. The individual dee voltages are used to set the balance capacitors which correct for side to side asymmetries. The resonator average voltages are used to tune the lower resonator so that the voltage is the same on both resonators and the average of the two resonator voltages is used as the automatic voltage control level.

The absolute voltage level was found by the x-ray end point method. A small electron source was mounted

in a hill and a copper target placed in the dee across the gap; the x-ray spectra were then measured with an intrinsic germanium x-ray spectrometer.

Cooling water flow rates in individual lines are not monitored but each line has a diode temperature indicator at a critical point. These temperatures are monitored and the interlock circuit is tripped by an overtemperature indication. Air cooling on the rf drive capacitor and balance capacitors is also monitored by temperature indicators.

7. Injection.- In the early stages of the cyclotron design, a simple analytic calculation was used to determine the optimum tandem voltage and ion charge states to maximize the cyclotron output beam current for seven ions over their full energy range. The calculation included constraints on the incoming ion rigidity and cyclotron induction to satisfy minimum stripping radius (145 mm) requirements. A selection of these results were shown to be in reasonable agreement with detailed orbit calculations. However, these calculations did not include acceleration at dee gap crossings and terminated on a static equilibrium orbit.

Detailed bounding injection trajectories for thirteen ions have now been calculated starting from a common point at the center of the injection dipole in the yoke wall through the initial turn in the cyclotron. The field maps obtained in 1979[6] were used in these calculations; the new maps discussed later are expected to introduce only minor perturbations.

The calculation is done iteratively. Starting with an analytic calculation of the injection energy and rf phase and no deflection at the dipole, an accelerated orbit code is used to calculate the trajectory and the transfer matrix to the stripping foil azimuth, and, after adjusting for the energy loss in the foil, the ion is accelerated at the new charge state for one turn in the cyclotron. The eccentricity of this turn gives the change in radius and radial momentum required at the stripping foil. The inverse matrix is constructed for these two parameters against the injection energy and injection angle to find the changes for the next iteration. The rf phase is sufficiently decoupled to permit its adjustment to be calculated independently. Normally three iterations are sufficient to calculate injection parameters for well centred accelerated orbits.

For the thirteen bounding cases calculated, the injection energy differed by at most 4% from the simple analytic calculations and the required injection dipole deflection varies from +9 to -14 mrad.

The injection dipole can deflect the most rigid incoming beam more than $\pm$ 60 mrad up to a midplane induction of 4.5 T but at $\langle B \rangle$ = 5.05 T, flux leakage from the cyclotron yoke shifts the injection dipole magnetization curve sufficiently to require operation at the extreme of its operating range to give the desired 10 mrad safety margin.

The injection dipole introduces a first harmonic component (B_1) in the cyclotron midplane. At R = 609 mm (near ν_R = 1), $\langle B \rangle$ = 5.05 T and maximum dipole excitation, B_1 = 0.12 mT - approximately one-sixth of the value calculated using the much simplified approximation that the near-saturated cyclotron yoke wall does not affect the flux distribution. The perturbation of 0.12 mT is small enough not to require compensation with the trim rods as originally planned.

Thirty-three 10 $\mu g/cm^2$ carbon stripping foils are mounted on a stainless steel "bicycle chain" that is threaded down the upper dee stem and along the middle of a dee. The foils can intercept the beam from a radius of 145 mm out to 265 mm; no azimuthal movement of the foils is required, allowing a simple mechanical assembly. Damaged foils are removed from the chain at the top of the cyclotron and replaced from a magazine containing 300 foils. Magazines can be replaced through a vacuum lock without losing the cyclotron midplane vacuum.

8. Trim Rods.- The magnetic field is isochronized with trim rods[4] - movable steel rods that extend from the top and bottom of the poles to the midplane surface of the hills. The rods are used as top-bottom pairs and locally decrease the midplane field when retracted. There are thirteen trim rods per hill, eight with 40 mm diameter and five with 60 mm diameter. The location, diameters and range of travel of the rods have been fixed for some time, but the mechanical design of the drive mechanisms has evolved considerably from the initial concept. Space limitations forced us to abandon individual motor drives and the thirteen rods in each quadrant are driven by three stepping motors through gears and clutches. The trim rods are staggered azimuthally on the hill (each overlaps its nearest neighbours radially) as shown in Fig. 6. The outermost trim rod on each hill will be used to create the first harmonic bump required for precessional extraction and this rod is driven directly by one of the stepping motors. The six rods along the upstream edge of the hill are driven by the second motor and the six along the downstream edge by the third motor. These latter two motors each drive a gear chain and the individual trim rods are connected to a gear by a T-bar clutch activated by a pneumatically driven piston. Only one of the six rods is driven at a time. Figure 7 is a photograph of the motor-gear-clutch assembly that drives the trim rods in one upper quadrant. Only one drive assembly was built to test operation in the fringing field that exceeds 100 mT at maximum excitation.

Fig. 6 The upper flutter pole assembly showing the 2 mm thick shims and the trim rod holes.

The trim rod retractions are set under computer control. The position of each rod is monitored by a linear potentiometer attached directly to the rod and read by a 12 bit ADC channel in the serial CAMAC highway. A keyboard command for a given retraction activates the correct stepping motor, engages the clutch and drives the rod to the requested position.

The stepping motors develop sufficient torque to drive the rods at all operating fields, but beyond <B> = 4.5 T the fringing field interfered with the operation of the solenoids that activate the pneumatic clutch drives and shielding had to be added around the solenoids (not shown in Fig. 7).

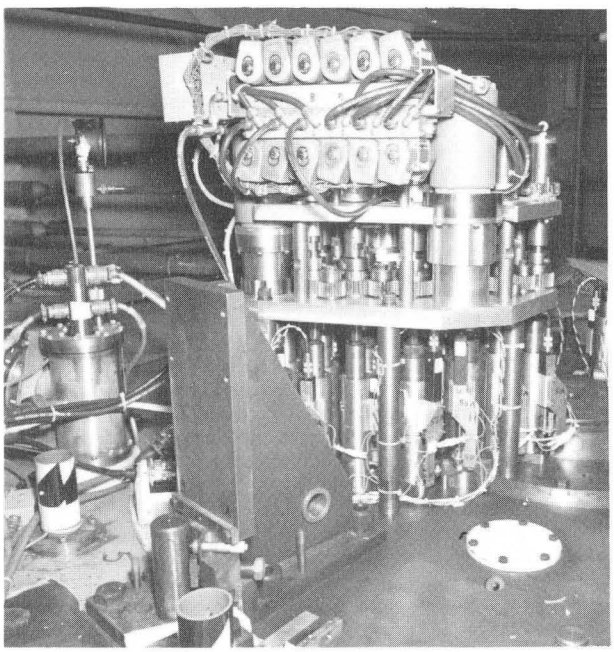

Fig. 7 The motor-gear-clutch assembly used to position the trim rods in one quadrant.

The dimples in the midplane field created by trim rod retractions differ slightly from what was expected, due mainly to the vestigial incremental magnetic susceptibility of the steel that is evident even beyond 4 T. These differences do not compromise the ability of the trim rods to isochronize the midplane field.

Figure 8 shows the measured peak dimple amplitude as a function of retraction of a 40 mm trim rod for four values of midplane induction. The 60 mm trim rods behave in a similar manner. The hill induction exceeds <B> by 1 T, so even for <B> = 1.2 T the trim rods are beyond the saturation magnetization of 2.14 μ_o^{-1} T. One should also note that two of the curves are below the minimum operating <B> of 2.5 T. The calculated dimple amplitude (using the uniform magnetization approximation) monotonically departs from the measured <B> = 4.6 T curve and exceeds it by 8% at maximum retraction.

At small retractions, the peak amplitude of the trim rod dimple increases with decreasing <B>. The greater susceptibility of the steel at lower <B> diverts more flux to the surrounding steel, enhancing the dimple amplitude and simultaneously increasing the induction several rod diameters away. At large retractions, the dimple amplitude is greater for larger midplane inductions but the radial extent of

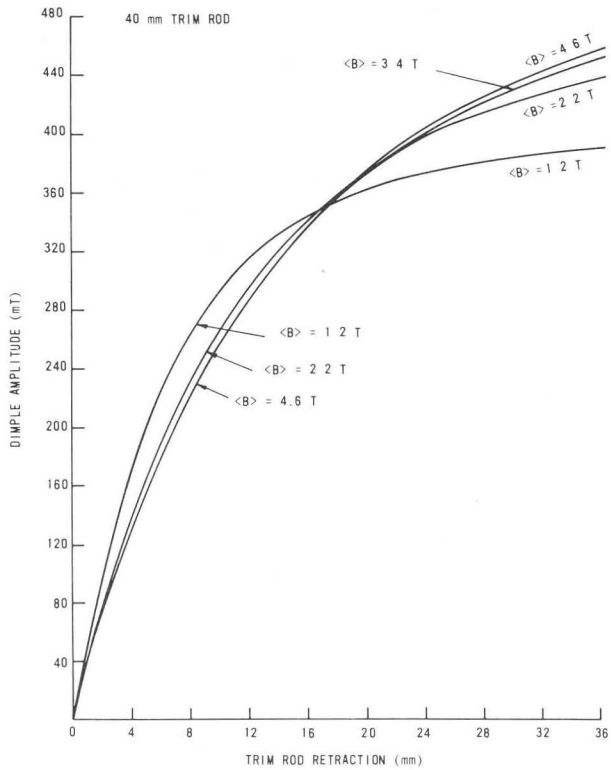

Fig. 8 Trim rod dimple amplitude as a function of retraction for four values of midplane induction.

the dimple is less. For the case of maximum retraction shown in Fig. 8, the peak amplitude for <B> = 4.6 T exceeds that for 1.2 T by 18%, but the total flux diverted is within 1% as determined from integrating over the entire dimple. The finite incremental susceptibiity also causes the dimple to depart slightly from axial symmetry in the direction nearest the azimuthal boundary of the flutter pole.

Over the radial range occupied by the trim rods, the flutter pole gap varies from 37 to 42 mm. Each rod is "zeroed" with its centre flush with the flutter pole surface, hence the variation of dimple amplitude with retraction is different for each of the thirteen sets of rods. Except for the unique response curve of each trim rod, the perturbations noted above have not been incorporated in the codes used to calculate the retractions necessary to create a given isochronous field. The method proposed to create such a field in actual operation is to start with calculated values near enough to permit acceleration to extraction with an acceptable phase slip (< 90°) then fine tune the field by further adjusting the trim rod retractions using the phase slip as measured with a movable phase probe. Examples of these isochronous fields are discussed below.

9. Magnetic Field Measurements.- The midplane field has been measured at 2° intervals using 40 flip coils that extend radially from 135 mm to 693 mm. The field beyond 693 mm has been measured by a single flip coil at 20 mm intervals along two secants through the cryostat where it is penetrated by the injection line and a probe hole. The coil and the two poles were centred to better than the required tolerance[5] for all these measurements.

Forty-eight midplane field maps comprise the main map library. Figure 9 shows the inner- and outer-coil currents used in the 6 x 8 skewed array. Lines of equal induction are also shown. Except for the six mapped points nearest the 5 T line, the excitations

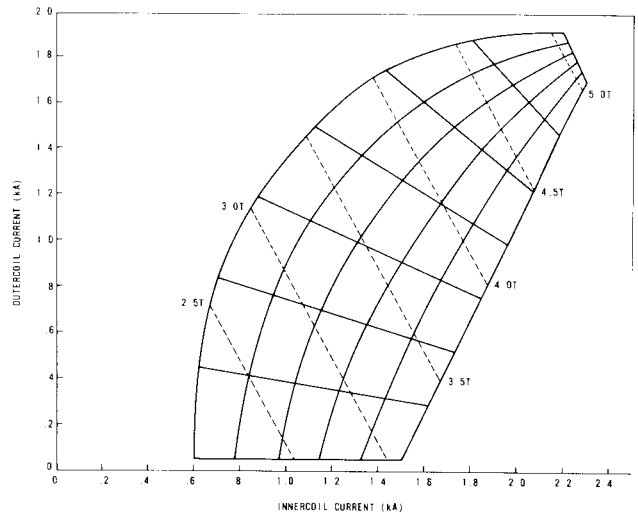

Fig. 9 Excitations used for the main map library. The 48 points where the solid lines intersect were mapped. The equi-induction lines are shown dashed.

are quite different from the initial library compiled in 1979[6]; the region where the coil lifted from the midplane bridge has been avoided and the mapped area extended towards the region of low outer-coil currents and high inner-coil currents to enclose the excitations required to accelerate the lightest ions to high specific energies.

The yoke steel configuration is different than it was when the first map library was taken; all 104 trim rods are now installed (compared to 24 and unbored flutter poles), shims (see Fig. 6) have been added to the flutter poles and some steel removed from the midplane surface at intermediate radii. For a given excitation, the additional trim rod steel adds an approximately uniform field difference whereas the flutter pole modifications increase the field at inner and outer radii and decrease it at intermediate radii.

The magnet exhibits some hysteresis. Two maps were made with identical currents to give <B> = 2.4 T - the first starting from zero excitation, the second from <B> = 4.6 T. The azimuthally averaged induction in the second map was greater by 2 mT at inner radii increasing to 2.9 mT near the pole's outer edge. This is approximately an order of magnitude greater than our reproducibility. In compiling the map library, each mapping point was approached from a lower excitation.

The midplane induction is a function of yoke temperature due to the variation in saturation magnetization. For the measurements shown in Fig. 10, the temperature in the cyclotron building was varied and the entire yoke brought to a uniform temperature for each measurement. Each point on the four curves is the average of five flip-coils (R = 377 to 437 mm) over the 180 azimuthal measurements, corrected for the flip-coils' temperature coefficient. These five flip coils were chosen because there is little radial

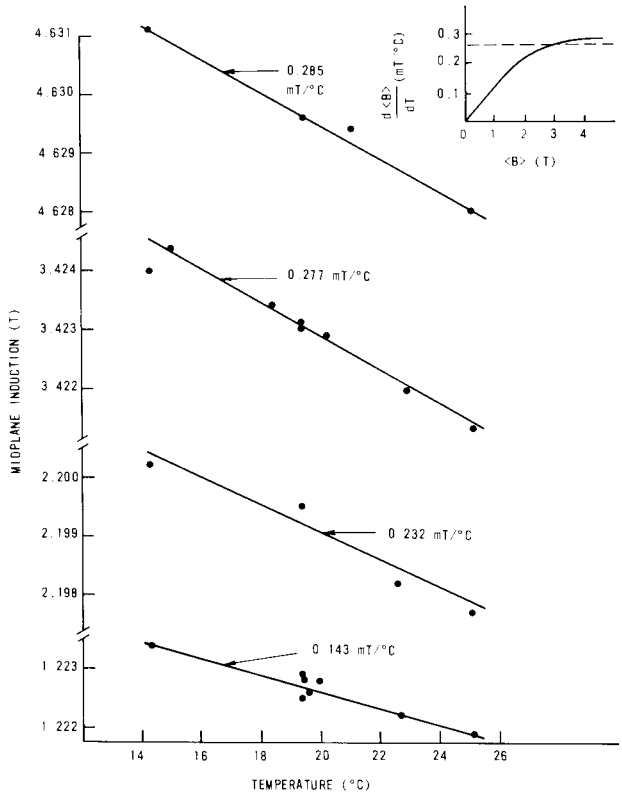

Fig. 10 The variation in midplane induction with temperature for four magnet excitations. The results are summarized in the insert where the dashed line is the expected asymptotic limit.

gradient in the average induction over that radial range, thus eliminating the need to correct for the radial variation of flip-coil position caused by the large temperature coefficient of the perspex rod that holds the flip coils.

As expected, the temperature coefficient of the midplane induction increases monotonically with increasing midplane induction and is summarized in the insert in the upper corner. The dashed line at 0.26 mT/°C is the expected asymptotic limit from the published value of 0.37 mT/°C[7] multiplied by the ratio of the midplane induction arising from the yoke steel to the saturation magnetization ($\mu_o M$ = 2.14 tesla). The measured value at 4.6 T exceeds this limit by ~ 10%. For the 48 maps in the main library, the cyclotron yoke was maintained at a temperature of 20.5 to 22.3°C.

The first and second harmonics in the midplane field maps are essentially the same as previously reported[6]. The first harmonic is less than 0.4 mT from the injection radius to ν_R = 1 and is nearly independent of midplane induction. It is caused mainly by manufacturing and alignment errors (within the tolerances) of the flutter pole assemblies and can easily be reduced by either small trim rod adjustments or modest shimming of the flutter poles. The second harmonic is caused mainly by the asymmetric midplane holes in the yoke wall and increases with increasing excitation. Even at full field it is everywhere less than 2.2 mT, well below tolerable limits and there is no need to compensate it.

10. Isochronous Fields.- Figure 11 shows the measured average midplane induction for accelerating iodine to 10 MeV/u, the resulting betatron frequencies calculated with a static orbit code and the phase slip calculated with an accelerated orbit code. The magnet coil currents were determined by a least squares interpolative fit within the 6 x 8 array of mapped fields shown in Fig. 9 and the trim rod retractions to isochronize the field were calculated from their measured response curves. The phase history of the beam could be improved by a further adjustment of the trim rods but the phase slip is already less than the probable phase error due to calibration errors in the flip coils (± 0.01%). The ripple in the betatron frequencies is mainly due to the trim rod corrections and is acceptably small everywhere.

Figure 12 shows the difference in the average midplane induction between the measured and "requested" values to accelerate carbon to 50 MeV/u. Also shown are the thirteen trim rod positions and their retractions. This is again for the initially calculated trim rod settings and results in a cumulative phase slip of only 30°. This is our most relativistic ion and requires quite large trim rod retractions; nevertheless, the phase slip is still small enough to

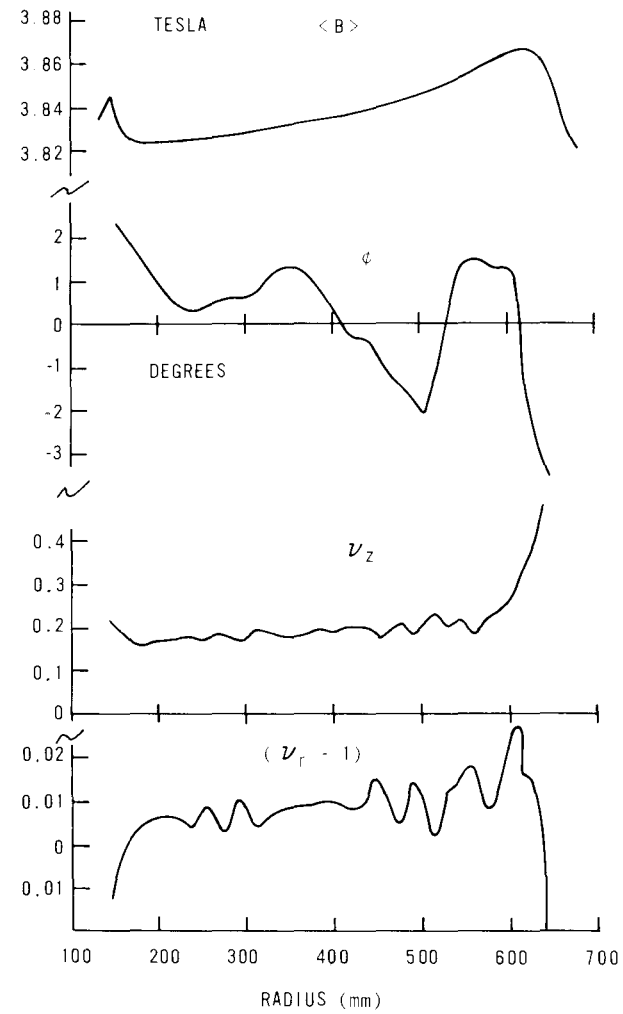

Fig. 11 The measured average midplane induction for accelerating I^{23+} to 10 MeV/u and the calculated phase slip and betatron frequencies using the measured field.

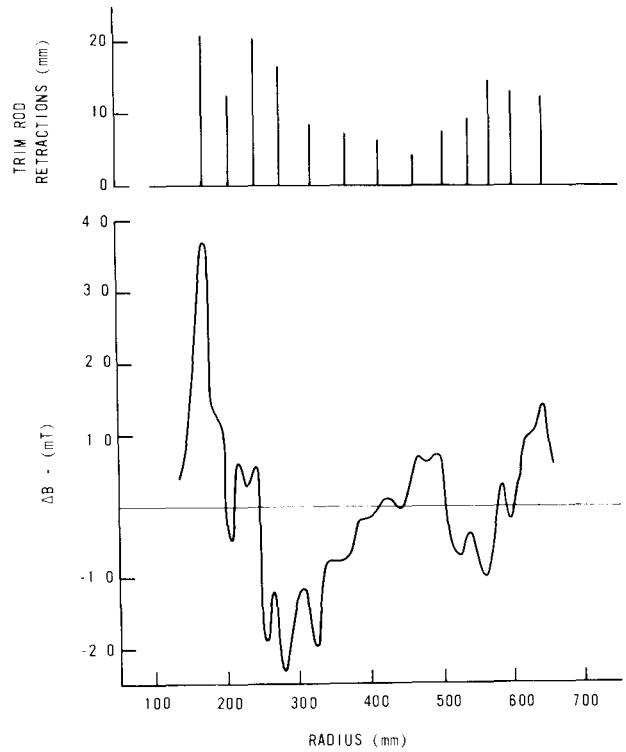

Fig. 12 The difference between the measured and "requested" midplane induction to accelerate C^{6+} to 50 MeV/u and the locations and retractions of the trim rods.

allow acceleration to extraction. As mentioned previously, final isochronization will be effected by further trim rod adjustments using a movable phase probe to determine the corrections. On the basis of these results, it is not essential to incorporate into the fitting codes the trim rod response perturbations due to midplane induction changes.

11. Extraction.- The extraction system consists of a single electrostatic deflector and a magnetic channel composed of both steel bars and superconducting windings.

A model electrostatic deflector system has been built and operated outside the cyclotron magnet. It has been used to develop high voltage components needed to couple a custom-made high voltage feed cable to the deflector electrode within the tight constraints imposed by the deflector being in a dee. Out-of-magnet operation exceeds design requirements of 100 kV across a 7 mm aperture. Testing in the magnet awaits installation of the rf system into the magnet.

Superconducting windings are used in the magnetic extraction elements to provide radial focusing and steering. Superconducting test coils have been made which model the radial focusing windings. These coils are wound from small cross section Nb_3Sn wire using the "wind-and-react" technique. Experiments show that the windings can carry the design current (300 A) in background magnetic fields which will arise at the radial focusing winding location in the cyclotron. Model coils to test the steering windings will also be studied. Details appear elsewhere in the proceedings[2].

12. Facility Status.- Successful operation of the magnet was demonstrated in 1978[1] at which time funds were requested to couple it to the tandem to make the integrated heavy-ion accelerator facility. Unfortunately, this coincided with a period of fiscal restraint and significant funding did not become available until 1980 April. Since then, appreciable progress has been made on all aspects of the facility.

The required new building construction is shown shaded in Fig. 1. It is scheduled to be enclosed this fall and service installation completed next summer. Construction of the control room extension has not yet started.

The order for the beam line magnets[8] was placed early last year when funds became available and the first delivery is due early next year. The rest will follow in sequence to match the installation schedule.

The present beam direction in the tandem is opposite to that shown in Fig. 1; reversing it requires rearrangement of the accelerating tubes but no change to the pressure vessel or charging system. The new ion source cage is under construction and installation will begin next year when the beam direction will be reversed.

The computer control system is a close copy of that developed for the VICKSI accelerator in Berlin[9]. A skeleton of the system has been in operation for three years and has already proved invaluable in field mapping, rf accelerating system experiments, trim rod operation and is now assuming control of the cryogenic system. Bulk ordering of CAMAC modules is in progress and the PDP 11-34 now being used will be replaced by two PDP 11-44s when the new control room is ready for occupancy.

The cyclotron magnet is to be transferred from the temporary building where it has been tested to the location shown in Fig. 1 next fall and the commissioning of the entire system is scheduled to start in the first half of 1983.

13. Acknowledgements.- It is a pleasure to acknowledge the able technical assistance of L.F. Birney, R.L. Burton, J.J. Hill, J.E. McGregor, R.E. Milks and J.F. Mouris and fruitful consultations with R.L. Graham, B.F. Greiner, L.G. Hansen and R.B. Walker on computer control.

References

1. J.H. ORMROD, C.B. BIGHAM, K.C. CHAN, E.A. HEIGHWAY, C.R. HOFFMANN, J.A. HULBERT, H.R. SCHNEIDER and Q.A. WALKER, IEEE Proc. NS-26 (1979) 2034.
2. C.R. HOFFMANN - these proceedings.
3. C.B. BIGHAM, IEEE Trans. NS-26 (1979) 2142.
4. C.B. BIGHAM, Nucl. Instr. & Methods 131 (1975) 223.
5. E.A. HEIGHWAY and K.R. CHAPLIN, Atomic Energy of Canada Limited, Report AECL-6079 (1977).
6. J.H. ORMROD, K.C. CHAN and J.J. HILL, Atomic Energy of Canada Limited, Report AECL-7161 (1980).
7. J.I. BUDNICK, L.J. BRUNER, R.J. BLUME and E.L. BOYD, J. Appl. Phys. 32 (1961) 1205.
8. W.G. DAVIES and A.R. RUTLEDGE, IEEE Trans. NS-26 (1979) 2086.
9. W. BUSSE and H. KLUGE, 7th Int. Conf. on Cyclotrons, Zurich, 1975, Birkhauser, p. 557.

" DISCUSSION "

C. BIETH : What is the dee voltage which has been measured on the test bench and the equivalent short circuit density ? What is the fast type of sliding contact which are used ?

J.H. ORMROD : The dees operate at 100 kV peak and the short circuit current is approximately 45 Amp/cm. The current sliding contacts are high conductivity copper alloy (CDA 155) that overlap azimuthally.